Hindawi
Discrete Dynamics in Nature and Society
Volume 2018, Article ID 5758324, 14 pages
https://doi.org/10.1155/2018/5758324

Research Article

Control of Chaos in a Single Machine Infinite Bus Power System Using the Discrete Sliding Mode Control Technique

Mohamed Zribi,[1] **Muthana T. Alrifai**,[1] **and Nejib Smaoui**[2]

[1]*Department of Electrical Engineering, Kuwait University, P.O. Box 5969, Safat 13060, Kuwait*
[2]*Department of Mathematics, Kuwait University, P.O. Box 5969, Safat 13060, Kuwait*

Correspondence should be addressed to Mohamed Zribi; mohamed.zribi10@gmail.com

Received 30 November 2017; Accepted 27 March 2018; Published 6 June 2018

Academic Editor: Victor S. Kozyakin

Under certain conditions, power systems may exhibit chaotic behaviors which are harmful and undesirable. In this paper, the discrete time sliding mode control technique is used to control a chaotic power system. The objective of the control is to eliminate the chaotic oscillations and to bring order to the power system. Two discrete time sliding mode control (DSMC) schemes are proposed for a fourth order discrete time chaotic power system. The first DSMC control scheme is based on the well-known exponential reaching law. The second DSMC control scheme is based on the recently developed double power reaching law. It is shown that the states of the controlled system converge to their desired values. Simulation results are presented for different values of the gains of the controllers as well as for different initial conditions. These results indicate that both control schemes work well. However, the simulation results show that the second control scheme gave better results since it was able to greatly reduce the chattering problem.

1. Introduction

Chaos in power systems was observed by [1, 2] over a range of loading conditions. Chaotic oscillations in power systems are harmful and undesirable. The increasing demand for electric power forces the power system to operate nearly close to its stability boundary. In this operating environment, a sudden disturbance can lead to a chaotic behavior [3–6]. Chaos is related to many power system instability phenomena such as voltage collapse which occurs when the power system is heavily loaded. Voltage collapse is characterized by a slow change in the operating point of the system caused by an increase in loads which results in a gradual decrease in voltage magnitudes until a sharp accelerated drop in voltage occurs. Voltage collapse can result in catastrophic blackouts [7–12]. Therefore, it is imperative to properly control the power system so that chaos is suppressed and chaotic oscillations are eliminated.

Chaos suppression in power systems has received the attention of many researchers. In recent years, many control methods were applied to suppress chaos and stabilize the voltage of the power systems [13–19]. Adaptive control was proposed in [13]. Fuzzy and neural control methods were discussed in [14–16]. Linear and nonlinear state feedback controllers are developed in [18] for the control of the bifurcation phenomenon in a power system A passivity-based adaptive controller was used in [19] to suppress chaotic oscillations in a power system.

Due to its simple implementation, good transient response, and robustness to parameters uncertainties and to disturbances, the sliding mode control technique has been applied to many nonlinear systems such as soft landing control, trajectory tracking, motor control, and power system control [20–25]. Power system chaos suppression using the sliding mode technique was proposed in the literature [26–28]. In [26], an approach that combines time scale separation design and sliding mode control was proposed. High order sliding mode controller was reported in [27]; the controller design was based on backstepping method.

As a result of the extensive use of computers in the implementation of controllers, discrete time sliding mode control has generated a sizable amount or research interest. There is subtle difference between continuous time sliding mode control and discrete time sliding mode control. For the DSMC, the control signal is determined once in every sampling interval and it is held constant during the sampling

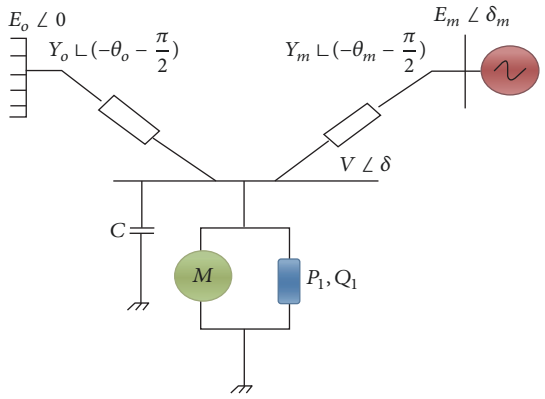

Figure 1: Schematic of a power system.

period [29–32]. Hence, we have the so-called quasi-sliding mode in DSMC. As a consequence, the design of discrete time sliding mode controllers needs to be carefully investigated.

This paper presents two discrete time sliding mode control schemes to eliminate chaos in a power system; the proposed DSMC control schemes use different reaching laws. The developed controllers are applied to a discretized 4th order three-bus power system model. Simulation studies clearly show that the proposed controllers work well.

The rest of the paper is organized as follows. The mathematical model of the power system is presented in Section 2; simulation results are also presented to show that the discretized model of the system displays chaotic behavior under certain loading conditions. The control problem is formulated in Section 3. The design of two discrete sliding mode control schemes for suppression of chaos is developed in Sections 4 and 5; simulation results for the controlled system are also presented and discussed in these sections. Finally, the conclusion is given in Section 6.

2. Modeling of the Power System

The power system studied in this paper is depicted in Figure 1; it consists of two generator buses and one load bus. One of the generator buses is an infinite busbar while the other generator bus has a constant voltage magnitude E_m. The Thevenin equivalent model representing the infinite busbar (external power system) is denoted by E_o, Y_o, and θ_o. The Thevenin equivalent model for the second generator (internal power system) is denoted by E_m, δ_m, Y_m, and θ_m. The load bus consists of an induction motor in parallel with a PQ load. Also, a fixed capacitor is added in parallel with the load to increase the voltage up to near one per unit. The magnitude of the load busbar voltage is denoted by V and phase angle of the load busbar voltage is denoted by δ.

The differential equation that describes the motion of the rotor of the synchronous generator can be written as follows:

$$M\ddot{\delta}_m + d_m\dot{\delta}_m = P_a = P_m - P_e, \tag{1}$$

where M is the momentum of inertia of the generator, d_m is a modified damping coefficient, P_a is the accelerating power, P_m is the input mechanical power, and P_e is the output electrical power.

The electric power P_e is given as

$$P_e = \mathrm{Re}\left(VI^*\right), \tag{2}$$

where V is the load busbar voltage and I^* is the complex conjugate of the current of the load busbar.

Referring to Figure 1, the equation of the electric power is as follows:

$$P_e = -E_m^2 Y_m \sin\left(\theta_m\right) - E_m V Y_m \sin\left(\delta - \delta_m + \theta_m\right), \tag{3}$$

where Y_m and θ_m are the magnitude and phase angle of the admittance between the second generator and the load busbar.

The induction motor is as proposed in [2]. Hence, the load model is described as follows:

$$\begin{aligned} P &= P_0 + P_1 + k_{pw}\dot{\delta} + k_{pv}\left(V + T\dot{V}\right), \\ Q &= Q_0 + Q_1 + k_{qw}\dot{\delta} + k_{qv}V + k_{qv2}V^2, \end{aligned} \tag{4}$$

where the constant real and reactive powers of the induction motor are P_0 and Q_0; the real and reactive components of the PQ load are P_1 and Q_1. The time constant of the motor is T. The constants parameters k_{pw}, k_{pv}, k_{qw}, k_{qv}, and k_{qv2} denote empirical constants that characterize the model of the load.

The real power supplied to the load bus by the network is as follows:

$$\begin{aligned} P = &-E_0' Y_0' V \sin\left(\delta + \theta_0'\right) - E_m Y_m V \sin\left(\delta - \delta_m + \theta_m\right) \\ &+ \left(Y_0' \sin\left(\theta_0\right) + Y_m \sin\left(\theta_m\right)\right) V^2, \end{aligned} \tag{5}$$

where E_0', Y_0', and θ_0' are the adjusted values of the Thevenin equivalent model of the infinite bus taking into account the added capacitor.

The reactive power supplied to the load bus by the network can be written as

$$\begin{aligned} Q = &E_0' Y_0' V \cos\left(\delta + \theta_0'\right) + E_m Y_m V \cos\left(\delta - \delta_m + \theta_m\right) \\ &- \left(Y_0' \cos\left(\theta_0\right) + Y_m \cos\left(\theta_m\right)\right) V^2. \end{aligned} \tag{6}$$

Hence, the dynamic model of the power system can be described as follows:

$$\begin{aligned} k_{qw}\dot{\delta} &= E_0' Y_0' V \cos\left(\delta + \theta_0'\right) + E_m Y_m V \cos\left(\delta - \delta_m \right. \\ &\left. + \theta_m\right) - k_{qv}V - Q_0 - Q_1 - \left(k_{qv2} + Y_0' \cos\left(\theta_0'\right)\right. \\ &\left. + Y_m \cos\left(\theta_m\right)\right) V^2, \\ T k_{qw} k_{pv} \dot{V} &= k_{pw} k_{qv2} V^2 + \left(k_{pw} k_{qv} - k_{qw} k_{pv}\right) V \\ &- k_{qw}\left(E_0' Y_0' V \sin\left(\delta + \theta_0'\right)\right. \end{aligned}$$

$$+ E_m Y_m V \sin\left(\delta - \delta_m + \theta_m\right)\Big) + k_{qw}\left(\left(Y_0' \sin\left(\theta_0'\right) + Y_m \sin\left(\theta_m\right)\right) V^2 - P_0 - P_1\right) - k_{pw}\left(E_0' Y_0' V \cos\left(\delta + \theta_0'\right) + E_m Y_m V \cos\left(\delta - \delta_m + \theta_m\right)\right) + k_{pw}\left(\left(Y_0' \cos\left(\theta_0'\right) + Y_m \cos\left(\theta_m\right)\right) V^2 + Q_0 + Q_1\right). \tag{7}$$

Also, δ_m is related to the generator rotor speed deviation ω such that

$$\dot{\delta}_m = \omega. \tag{8}$$

Using (1), (3), and (8), we get

$$M\dot{\omega} = -d_m\omega + P_m + E_m V Y_m \sin\left(\delta - \delta_m - \theta_m\right) + E_m^2 Y_m \sin\left(\theta_m\right). \tag{9}$$

Using (7), (8), and (9), the model of the fourth order power system can be written as follows:

$$\begin{aligned}
k_{qw}\dot{\delta} &= E_0' Y_0' V \cos\left(\delta + \theta_0'\right) + E_m Y_m V \cos\left(\delta - \delta_m + \theta_m\right) - k_{qv} V - Q_0 - Q_1 - \left(k_{qv2} + Y_0' \cos\left(\theta_0'\right) + Y_m \cos\left(\theta_m\right)\right) V^2,\\
Tk_{qw}k_{pv}\dot{V} &= k_{pw}k_{qv2}V^2 + \left(k_{pw}k_{qv} - k_{qw}k_{pv}\right) V - k_{qw}\left(E_0' Y_0' V \sin\left(\delta + \theta_0'\right) + E_m Y_m V \sin\left(\delta - \delta_m + \theta_m\right)\right) + k_{qw}\left(\left(Y_0' \sin\left(\theta_0'\right) + Y_m \sin\left(\theta_m\right)\right) V^2 - P_0 - P_1\right)\\
&\quad - k_{pw}\left(E_0' Y_0' V \cos\left(\delta + \theta_0'\right) + E_m Y_m V \cos\left(\delta - \delta_m + \theta_m\right)\right) + k_{pw}\left(\left(Y_0' \cos\left(\theta_0'\right) + Y_m \cos\left(\theta_m\right)\right) V^2 + Q_0 + Q_1\right),\\
\dot{\delta}_m &= \omega,\\
M\dot{\omega} &= -d_m\omega + P_m + E_m V Y_m \sin\left(\delta - \delta_m - \theta_m\right) + E_m^2 Y_m \sin\left(\theta_m\right).
\end{aligned} \tag{10}$$

Define the state variables x_1, x_2, x_3, and x_4 such that $x_1 = \delta$, $x_2 = V$, $x_3 = \delta_m$, and $x_4 = \omega$. Also, recall that Q_1 is a system parameter representing the reactive power in the system.

The parameters of the power system are obtained from [2]. The parameters of the generator are such that $M = 0.3$, $d_m = 0.05$, $P_m = 1$, $E_m = 1$, $Y_m = 5$, and $\theta_m = -5$. The parameters of the network are such that $E_0 = 1$, $Y_0 = 20$, $\theta_0 = -5$, $E_0' = 2.5$, $Y_0' = 8$, and $\theta_0' = -12$. The empirical constants of the load are such that $k_{pw} = 0.4$, $k_{pv} = 0.3$, $k_{qw} = -0.03$, $k_{qv} = -2.8$, $k_{qv2} = 2.1$, $T = 8.5$, $P_0 = 0.6$, $Q_0 = 1.3$, $P_1 = 0.0$, and $C = 12$. All the parameters values are in per unit except the angles which are in degrees.

Then, the equations of the power system given by (10) can be written in compact form as follows:

$$\begin{aligned}
\dot{x}_1 &= c_1 x_2^2 - c_2 x_2 \cos\left(x_1 - x_3 - c_3\right) - c_4 x_2 \cos\left(x_1 - c_5\right) - c_6 x_2 + c_7 Q_1 + c_8,\\
\dot{x}_2 &= -c_9 x_2^2 + c_{10} x_2 \cos\left(x_1 - x_3 - c_{11}\right) + c_{12} x_2 \cos\left(x_1 - c_{13}\right) + c_{14} x_2 - c_{15} Q_1 - c_{16},\\
\dot{x}_3 &= x_4,\\
\dot{x}_4 &= c_{17} x_2 \sin\left(x_1 - x_3 + c_3\right) - c_{18} x_4 + c_{19},
\end{aligned} \tag{11}$$

where the parameters c_1–c_{19} are such that $c_1 = 496.8718$, $c_2 = 166.666667$, $c_3 = 0.08727$, $c_4 = 666.66667$, $c_5 = 0.20944$, $c_6 = 93.3333$, $c_7 = 33.33333$, $c_8 = 43.33333$, $c_9 = 78.76384$, $c_{10} = 26.21722$, $c_{11} = 0.011241$, $c_{12} = 104.86887$, $c_{13} = 0.13458$, $c_{14} = 14.52288$, $c_{15} = 5.2288$, $c_{16} = 7.03268$, $c_{17} = 16.66667$, $c_{18} = 0.16667$, and $c_{19} = 1.88074$.

This paper deals with the design of discrete time sliding mode control schemes to suppress chaos present in the power system. Therefore, the continuous time model of the system given by (11) is discretized using the Euler method. The discretized dynamic model of the power system is as follows:

$$\begin{aligned}
x_1(k+1) &= x_1(k) + a_1 x_2^2(k) - a_2 x_2(k) \cos\left(x_1(k) - x_3(k) - a_3\right) - a_4 x_2(k) \cos\left(x_1(k) - a_5\right) - a_6 x_2(k) + a_7 Q_1 + a_8,\\
x_2(k+1) &= -a_9 x_2^2(k) + a_{10} x_2(k) \cos\left(x_1(k) - x_3(k) - a_{11}\right) + a_{12} x_2(k) \cos\left(x_1(k) - a_{13}\right) + a_{14} x_2(k) - a_{15} Q_1 - a_{16},\\
x_3(k+1) &= x_3(k) + T_s x_4(k),\\
x_4(k+1) &= x_4(k) + a_{17} x_2(k) \sin\left(x_1(k) - x_3(k) + a_3\right) - a_{18} x_4(k) + a_{19},
\end{aligned} \tag{12}$$

where $a_1 = 496.8718T_s$, $a_2 = 166.666667T_s$, $a_3 = 0.08727$, $a_4 = 666.66667T_s$, $a_5 = 0.20944$, $a_6 = 93.3333T_s$, $a_7 = 33.33333T_s$, $a_8 = 43.33333T_s$, $a_9 = 78.76384T_s$, $a_{10} = 26.21722T_s$, $a_{11} = 0.011241$, $a_{12} = 104.86887T_s$, $a_{13} = 0.13458$, $a_{14} = 14.52288T_s + 1$, $a_{15} = 5.2288T_s$, $a_{16} = 7.03268T_s$, $a_{17} = 16.66667T_s$, $a_{18} = 0.16667T_s$, and $a_{19} = 1.88074T_s$. Note that $T_s > 0$ is the sampling period.

For $Q_1 = 11.379$, the discretized model of the power system given by (12) has Lyapunov exponents: $\lambda_1 = 0.2793$,

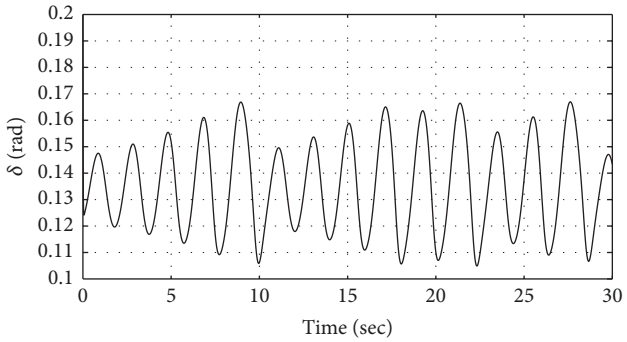

Figure 2: The load phase angle versus time without control.

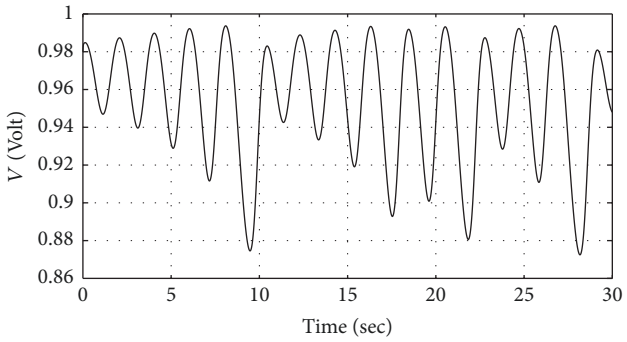

Figure 3: The load voltage versus time without control.

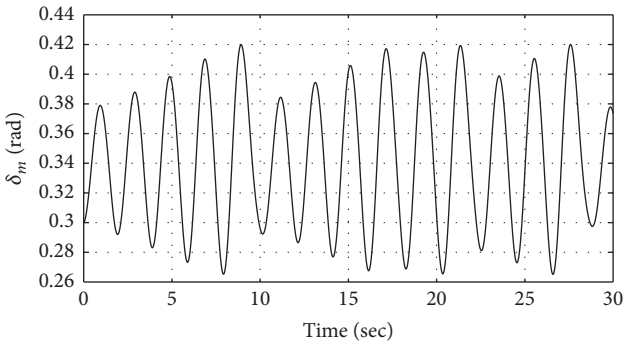

Figure 4: The generator phase angle versus time without control.

$\lambda_2 = 0.001 \approx 0$, $\lambda_3 = -4.24$, and $\lambda_4 = -100.74$. Since there is one positive Lyapunov exponent, two negative Lyapunov exponents, and one Lyapunov exponent which is approximately zero, then it can be concluded that the discretized model of the power system (12) is chaotic when $Q_1 = 11.379$.

In addition, the discretized model of the power system (12) is simulated using the MATLAB software. The simulation results are presented in Figures 2–9. Figures 2–5 show the trajectories of the load phase angle versus time, the load voltage versus time, the generator phase angle versus time, and the generator rotor speed deviation versus time, respectively. Also, 3D plots of the states of the system are shown in Figures 6–9. Hence, the simulation results clearly show that the discretized model of the power system given by (12) is indeed chaotic when $Q_1 = 11.379$.

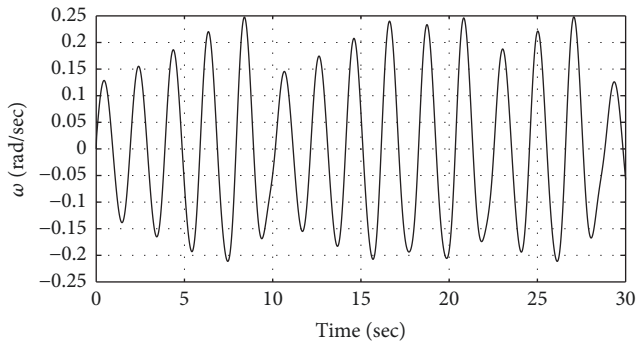

Figure 5: The generator rotor speed deviation versus time without control.

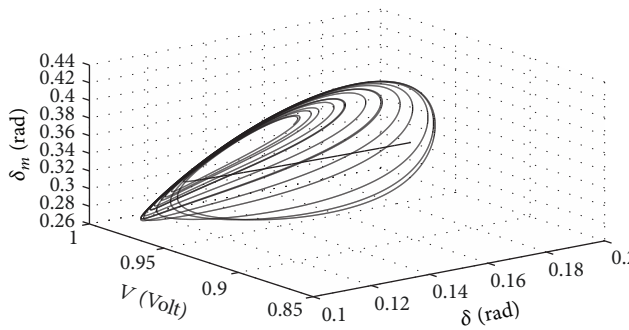

Figure 6: The 3D graph of δ-V-δ_m without control.

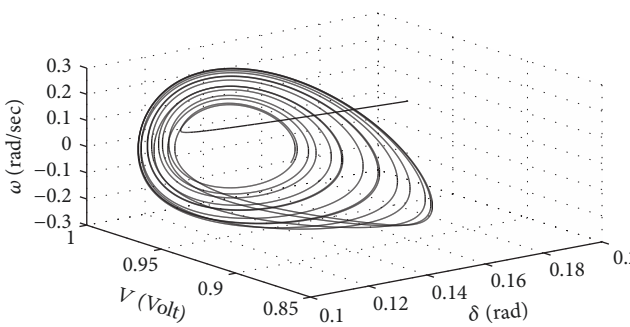

Figure 7: The 3D graph of δ-V-ω without control.

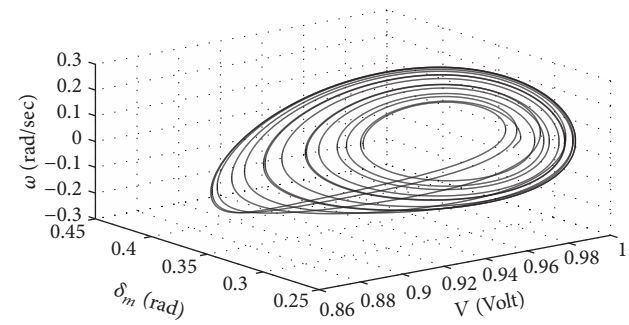

Figure 8: The 3D graph of V-δ_m-ω without control.

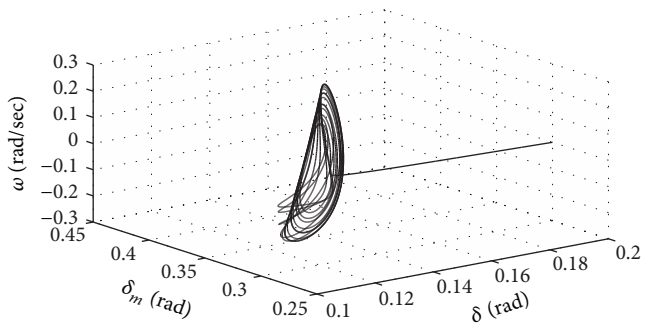

Figure 9: The 3D graph of δ-δ_m-ω without control.

3. Problem Formulation

The objective of this paper is to drive the states of the system $x_1 = \delta$, $x_2 = V$, $x_3 = \delta_m$, and $x_4 = \omega$ to their desired constant values x_{1d}, x_{2d}, x_{3d}, and x_{4d}, respectively. Note that the desired value of $x_4 = \omega$ should be zero; that is, $x_{4d} = 0$. We will denote by x_d the vector of desired values such that $x_d = \begin{bmatrix} x_{1d} & x_{2d} & x_{3d} & x_{4d} \end{bmatrix}^T$.

To be able to control the discretized model of the chaotic power system in (12), control inputs need to be added to the system. Adding control inputs to the first, the second, and the fourth difference equations of the system, the discretized dynamic model of the power system with control inputs is such that

$$\begin{aligned}
x_1(k+1) &= x_1(k) + a_1 x_2^2(k) \\
&\quad - a_2 x_2(k) \cos\left(x_1(k) - x_3(k) - a_3\right) \\
&\quad - a_4 x_2(k) \cos\left(x_1(k) - a_5\right) - a_6 x_2(k) \\
&\quad + a_7 Q_1 + a_8 + u_1(k), \\
x_2(k+1) &= -a_9 x_2^2(k) \\
&\quad + a_{10} x_2(k) \cos\left(x_1(k) - x_3(k) - a_{11}\right) \\
&\quad + a_{12} x_2(k) \cos\left(x_1(k) - a_{13}\right) \\
&\quad + a_{14} x_2(k) - a_{15} Q_1 - a_{16} + u_2(k), \\
x_3(k+1) &= x_3(k) + T_s x_4(k), \\
x_4(k+1) &= x_4(k) \\
&\quad + a_{17} x_2(k) \sin\left(x_1(k) - x_3(k) + a_3\right) \\
&\quad - a_{18} x_4(k) + a_{19} + u_3(k).
\end{aligned} \tag{13}$$

Define the regulation error vector $e(k) = \begin{bmatrix} e_1(k) & e_2(k) & e_3(k) & e_4(k) \end{bmatrix}^T$ such that $e(k) = x(k) - x_d$, or

$$e(k) = \begin{bmatrix} e_1(k) \\ e_2(k) \\ e_3(k) \\ e_4(k) \end{bmatrix} = \begin{bmatrix} x_1(k) - x_{1d} \\ x_2(k) - x_{2d} \\ x_3(k) - x_{3d} \\ x_4(k) \end{bmatrix}. \tag{14}$$

Using (13) and (14), the error dynamic model of the power system can be written as follows:

$$\begin{aligned}
e_1(k+1) &= e_1(k) + a_1 \left(e_2(k) + x_{2d}\right)^2 \\
&\quad - a_2 \left(e_2(k) + x_{2d}\right) \\
&\quad \cdot \cos\left(e_1(k) + x_{1d} - e_3(k) - x_{3d} - a_3\right) \\
&\quad - a_4 \left(e_2(k) + x_{2d}\right) \cos\left(e_1(k) + x_{1d} - a_5\right) \\
&\quad - a_6 \left(e_2(k) + x_{2d}\right) + a_7 Q_1 + a_8 + u_1(k), \\
e_2(k+1) &= -x_{2d} - a_9 \left(e_2(k) + x_{2d}\right)^2 \\
&\quad + a_{10} \left(e_2(k) + x_{2d}\right) \\
&\quad \cdot \cos\left(e_1(k) + x_{1d} - e_3(k) - x_{3d} - a_{11}\right) \\
&\quad + a_{12} \left(e_2(k) + x_{2d}\right) \cos\left(e_1(k) + x_{1d} - a_{13}\right) \\
&\quad + a_{14} \left(e_2(k) + x_{2d}\right) - a_{15} Q_1 - a_{16} + u_2(k), \\
e_3(k+1) &= e_3(k) + T_s e_4(k), \\
e_4(k+1) &= e_4(k) + a_{17} \left(e_2(k) + x_{2d}\right) \\
&\quad \cdot \sin\left(e_1(k) + x_{1d} - e_3(k) - x_{3d} + a_3\right) - a_{18} e_4(k) \\
&\quad + a_{19} + u_3(k).
\end{aligned} \tag{15}$$

Two DSMC schemes will be designed to drive the states of the system δ, V, δ_m, and ω, to converge to their desired constant values x_{1d}, x_{2d}, x_{3d}, and x_{4d}, respectively. This is done by forcing the error vector $e(k)$ to converge to $(0, 0, 0, 0)$. The design of the two control schemes will be discussed in detail in the next two sections.

4. A DSMC Scheme Based on the Exponential Reaching Law

4.1. Design of the Controller. The first step in the design of a sliding mode controller is the choice of the sliding surfaces. Since the system has three control inputs, we need to choose three sliding surfaces. The sliding surfaces $S_1(k)$, $S_2(k)$, and $S_3(k)$ are chosen such that

$$\begin{aligned}
S_1(k) &= e_1(k), \\
S_2(k) &= e_2(k), \\
S_3(k) &= (1 - \gamma) e_3(k) + T_s e_4(k),
\end{aligned} \tag{16}$$

where γ is a positive design parameter such that $|\gamma| < 1$.

Also, define the sgn function such that

$$\operatorname{sgn}(S_i) = \begin{cases} 1 & \text{if } S_i > 0 \\ 0 & \text{if } S_i = 0 \\ -1 & \text{if } S_i < 0. \end{cases} \tag{17}$$

Let the positive parameters q, ϵ, and T_s be such that $1 - qT_s > 0$. Proposition 1 gives the first discrete sliding mode control scheme.

Proposition 1. *The following sliding mode control controller*

$$\begin{aligned}
u_1(k) &= (1 - qT_s) S_1(k) - \varepsilon T_s \operatorname{sgn}(S_1(k)) - e_1(k) \\
&\quad - a_1 (e_2(k) + x_{2d})^2 + a_2 (e_2(k) + x_{2d}) \\
&\quad \cdot \cos(e_1(k) + x_{1d} - e_3(k) - x_{3d} - a_3) \\
&\quad + a_4 (e_2(k) + x_{2d}) \cos(e_1(k) + x_{1d} - a_5) \\
&\quad + a_6 (e_2(k) + x_{2d}) - a_7 Q_1 - a_8, \\
u_2(k) &= (1 - qT_s) S_2(k) - \varepsilon T_s \operatorname{sgn}(S_2(k)) + x_{2d} \\
&\quad + a_9 (e_2(k) + x_{2d})^2 - a_{10} (e_2(k) + x_{2d}) \\
&\quad \cdot \cos(e_1(k) + x_{1d} - e_3(k) - x_{3d} - a_{11}) \\
&\quad - a_{12} (e_2(k) + x_{2d}) \cos(e_1(k) + x_{1d} - a_{13}) \\
&\quad - a_{14} (e_2(k) + x_{2d}) + a_{15} Q_1 + a_{16} \\
&\quad + a_9 (e_2(k) + x_{2d})^2, \\
u_3(k) &= \frac{1}{T_s} \left((1 - qT_s) S_3(k) - \varepsilon T_s \operatorname{sgn}(S_3(k)) \right) \\
&\quad + \frac{\gamma - 1}{T_s} (e_3(k) + T_s e_4(k)) - e_4(k) \\
&\quad - a_{17} (e_2(k) + x_{2d}) \\
&\quad \cdot \sin(e_1(k) + x_{1d} - e_3(k) - x_{3d} + a_3) + a_{18} e_4(k) \\
&\quad - a_{19}
\end{aligned} \tag{18}$$

when applied to the discretized model of the power system (13) guarantees the convergence of the states of the system to their desired values.

Proof. Using the sliding surfaces given by (16), the dynamical model of the errors in (15), and the control scheme given by (18), we obtain

$$\begin{aligned}
S_1(k+1) &= e_1(k+1) = e_1(k) + a_1 (e_2(k) + x_{2d})^2 \\
&\quad - a_2 (e_2(k) + x_{2d}) \\
&\quad \cdot \cos(e_1(k) + x_{1d} - e_3(k) - x_{3d} - a_3) \\
&\quad - a_4 (e_2(k) + x_{2d}) \cos(e_1(k) + x_{1d} - a_5) \\
&\quad - a_6 (e_2(k) + x_{2d}) + a_7 Q_1 + a_8 + u_1(k) \\
&\quad = (1 - qT_s) S_1(k) - \epsilon T_s \operatorname{sgn}(S_1(k)), \\
S_2(k+1) &= e_2(k+1) = -x_{2d} - a_9 (e_2(k) + x_{2d})^2 \\
&\quad + a_{10} (e_2(k) + x_{2d}) \\
&\quad \cdot \cos(e_1(k) + x_{1d} - e_3(k) - x_{3d} - a_{11}) \\
&\quad + a_{12} (e_2(k) + x_{2d}) \cos(e_1(k) + x_{1d} - a_{13}) \\
&\quad + a_{14} (e_2(k) + x_{2d}) - a_{15} Q_1 - a_{16} + u_2(k) \\
&\quad = (1 - qT_s) S_2(k) - \epsilon T_s \operatorname{sgn}(S_2(k)), \\
S_3(k+1) &= (1 - \gamma) e_3(k+1) + T_s e_4(k+1) = (1 - \gamma) \\
&\quad \cdot (e_3(k) + T_s e_4(k)) \\
&\quad + T_s (e_4(k) + -a_{18} e_4(k) + a_{19} + u_3(k)) \\
&\quad + T_s a_{17} (e_2(k) + x_{2d}) \\
&\quad \cdot \sin(e_1(k) + x_{1d} - e_3(k) - x_{3d} + a_3) = (1 - qT_s) \\
&\quad \cdot S_3(k) - \epsilon T_s \operatorname{sgn}(S_3(k)).
\end{aligned} \tag{19}$$

Therefore, (19) can be written as follows:

$$S_i(k+1) = (1 - qT_s) S_i(k) - \epsilon T_s \operatorname{sgn}(S_i(k)) \quad (i = 1, 2, 3). \tag{20}$$

Sarpturk et al. [33] showed that a necessary and sufficient condition assuring both sliding motion and convergence onto the ith hyperplane may be stated as

$$|S_i(k+1)| < |S_i(k)|. \tag{21}$$

The condition given by (21) guarantees that all the trajectories will enter and remain within a domain of decreasing or at the worst case nonincreasing radius. The inequality in (21) can be decomposed into the following two inequalities:

$$(S_i(k+1) - S_i(k)) \operatorname{sgn}(S_i(k)) < 0, \tag{22}$$

$$(S_i(k+1) + S_i(k)) \operatorname{sgn}(S_i(k)) > 0. \tag{23}$$

Conditions (22) and (23) result in a lower bound and in an upper bound for the control action, respectively. While condition (22) implies that the closed-loop system should be moving in the direction of the sliding surface, condition (23) implies that the closed-loop system is not allowed to go too far in that direction.

Moreover, it was shown by Gao et al. [34] that the discrete system given by (20) meets the existence and the reaching condition $|S_i(k+1)| < |S_i(k)|$. Also, it was specified in [34] that the system given by (20) has the following properties. (1) Starting from any initial condition, the trajectories of system (20) will move toward the switching surface and cross it in finite time. (2) After crossing the switching surface, the trajectories of system (20) will cross the plane again in every successive sampling period, resulting in a zigzag motion about the switching surface. The size of each successive zigzag step is nonincreasing and the trajectories stay within a specified band called the quasi-sliding band.

It was stated in [34] that the quasi-sliding band (QSMB) is given by

$$\left\{ x : |S(x)| < \frac{\epsilon T_s}{2 - qT_s} \right\}. \tag{24}$$

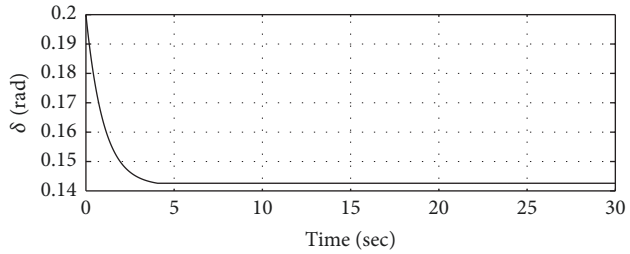

Figure 10: The load phase angle versus time using the first control law (case 1).

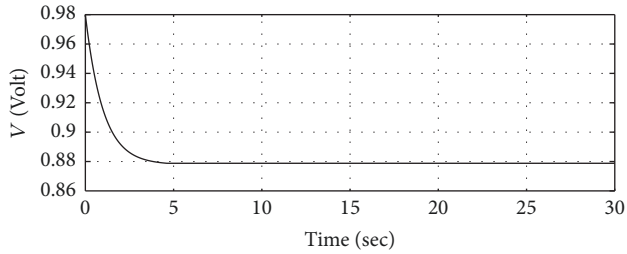

Figure 11: The load voltage versus time using the first control law (case 1).

Also, the width of the QSMB is

$$2\Delta = \frac{2\epsilon T_s}{2 - qT_s}. \tag{25}$$

It is worth mentioning that a desirable reaching mode response can be achieved by adjusting the parameters ϵ and q.

Therefore, it can be concluded that since $S_1(k)$, $S_2(k)$, and $S_3(k)$ satisfy (20), they will reach zero in finite time.

On the sliding surface, $S_1(k) = 0$, we have

$$e_1(k) = 0. \tag{26}$$

On the sliding surface, $S_2(k) = 0$, we have

$$e_2(k) = 0. \tag{27}$$

On the sliding surface, $S_3(k) = 0$, we have

$$e_3(k) + T_s e_4(k) = \gamma e_3(k). \tag{28}$$

Using the difference equation given by (28) and the third difference equation of the error system (15), we can write $e_3(k+1) = e_3(k) + T_s e_4(k) = \gamma e_3(k)$. Thus, $e_3(k)$ asymptotically converges to zero as $k \to \infty$ since $|\gamma| < 1$. Also, using (28), it is clear that $e_4(k)$ will converge to zero asymptotically as k tends to infinity.

Therefore, the errors $e_1(k)$, $e_2(k)$, $e_3(k)$, and $e_4(k)$ converge to zero. The convergence of the errors $e_1(k), e_2(k), e_3(k)$, and $e_4(k)$ to zero guarantees that $x_1(k)$, $x_2(k)$, $x_3(k)$, and $x_4(k)$ converge to their desired values x_{1d}, x_{2d}, x_{3d}, and x_{4d}, respectively, as $k \to \infty$. □

4.2. Simulation Results. The designed sliding mode controller in (18) is applied to the discretized model of the chaotic power system given by (13). The performance of the controlled system is simulated using the MATLAB/SIMULINK software. The parameters of the system are taken from [2]. In the simulation, the initial states are taken to be $\delta(0) = 0.2$, $V(0) = 0.97$, $\delta_m(0) = 0.3$, and $\omega(0) = 0$. The desired states are taken to be $x_{1d} = 0.1426$, $x_{2d} = 0.8788$, $x_{3d} = 0.3587$, and $x_{4d} = 0$. The sampling time T_s is taken to be $T_s = 0.001$. We simulated the performances of the controlled power system for 3 different cases. For the first case, the parameters of the controller are taken to be $q = 1$, $\epsilon = 0.001$, and $\gamma = 0.1$. The simulation results are shown in Figures 10–17. Figures 10–13

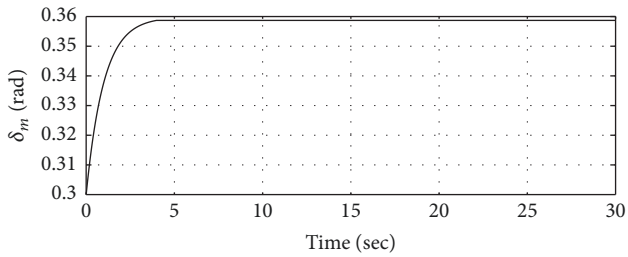

Figure 12: The generator phase angle versus time using the first control law (case 1).

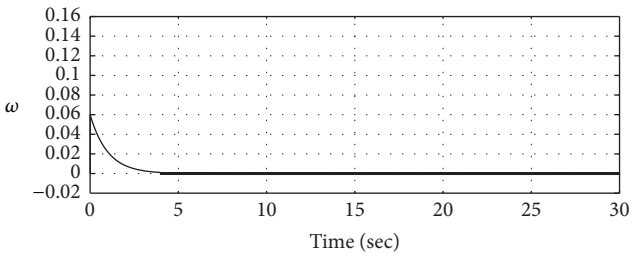

Figure 13: The generator rotor speed deviation versus time using the first control law (case 1).

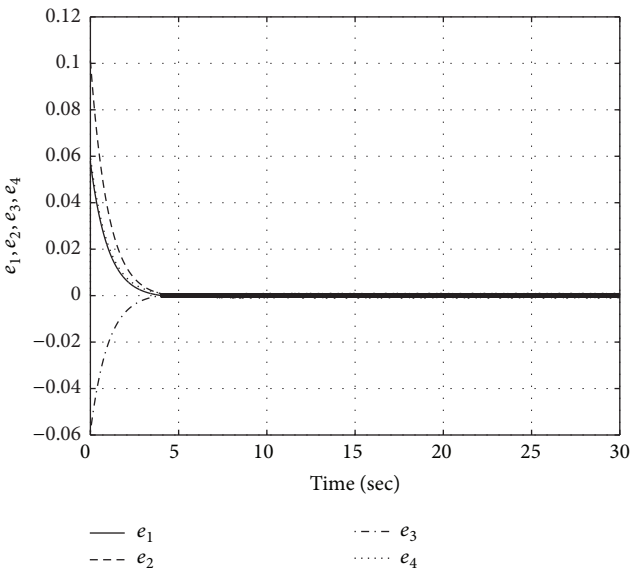

Figure 14: The errors versus time using the first control law (case 1).

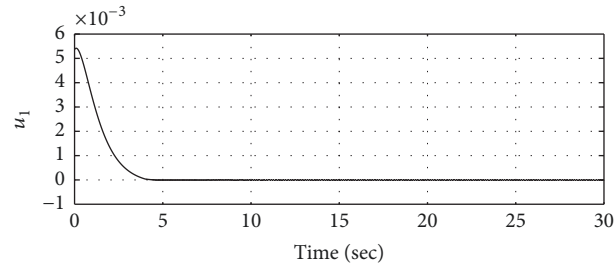

Figure 15: The controller u_1 versus time using the first control law (case 1).

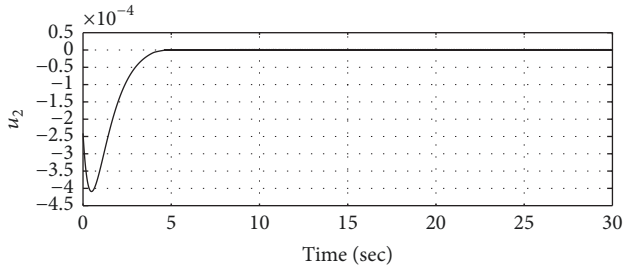

Figure 16: The controller u_2 versus time using the first control law (case 1).

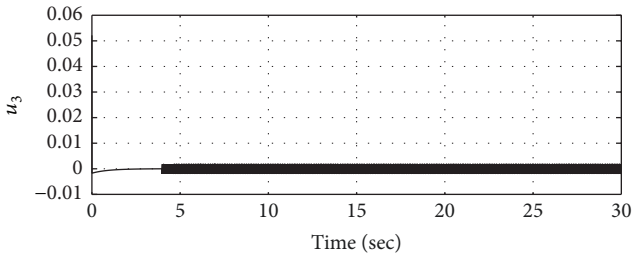

Figure 17: The controller u_3 versus time using the first control law (case 1).

show the trajectories of the load phase angle versus time, the load voltage versus time, the generator phase angle versus time, and the generator rotor speed deviation versus time. The errors versus time are shown in Figure 14. It is clear that the errors converge to zero in about 5 seconds. Therefore, it can be concluded that the proposed discrete sliding mode controller is able to suppress chaos in the power system. In addition, the controllers u_1, u_2, and u_3 versus time are presented in Figures 15–17. It is clear that some of the trajectories of the system as well as the controllers display a zigzag motion of the trajectories about the switching surfaces; the magnitude of the zigzag motion is higher for the generator rotor speed deviation and for the control law u_3. For the second case, the parameters of the controller are taken to be $q = 5$, $\epsilon = 0.01$, and $\gamma = 0.1$. The simulation results are shown in Figures 18–22. Figures 18–21 show the trajectories of the load phase angle versus time, the load voltage versus time, the generator phase angle versus time, and the generator rotor speed deviation versus time. The errors versus time are shown in Figure 22. It is clear that the errors converge to zero in

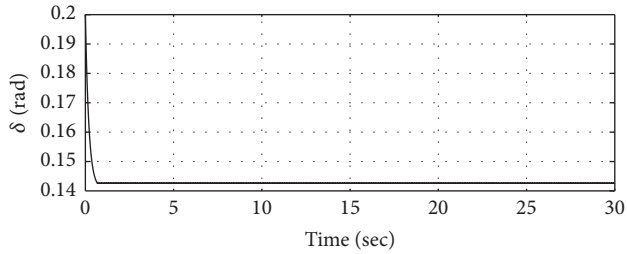

Figure 18: The load phase angle versus time using the first control law (case 2).

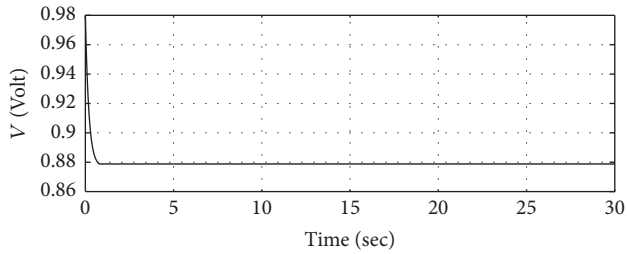

Figure 19: The load voltage versus time using the first control law (case 2).

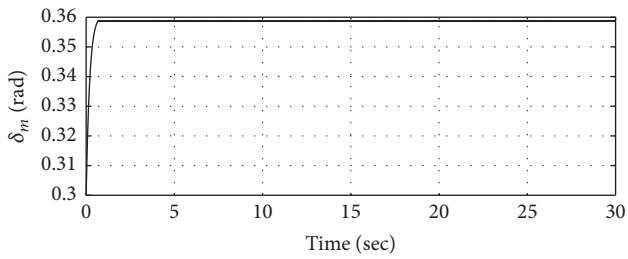

Figure 20: The generator phase angle versus time using the first control law (case 2).

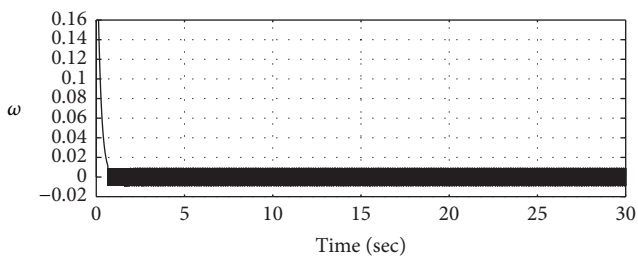

Figure 21: The generator rotor speed deviation versus time using the first control law (case 2).

less than one second. It is noted that the response of the system is faster than the previous case. However, some of the trajectories of the system display a zigzag motion of the trajectories about the switching surfaces; the magnitude of the zigzag motion is higher for the generator rotor speed deviation. For the third case, the parameters of the controller are taken to be $q = 1$, $\epsilon = 0.001$, and $\gamma = 0.1$. However, the initial condition of $\omega(t)$ is taken to be $\omega(0) = 0.2$. It is well known that chaotic systems are very sensitive to

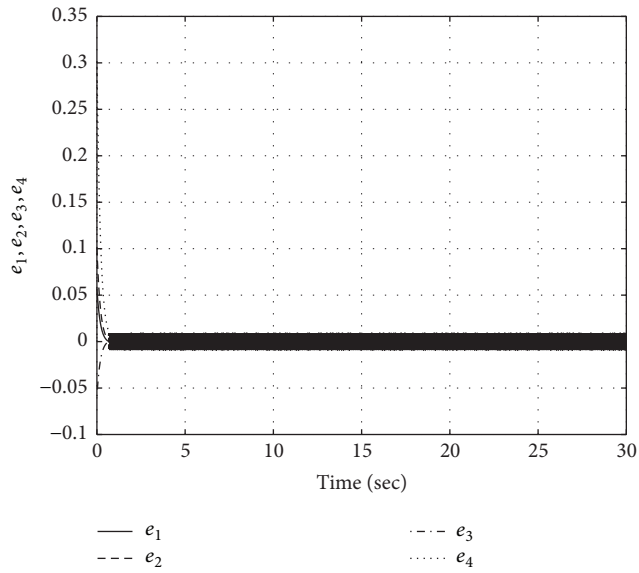

Figure 22: The errors versus time using the first control law (case 2).

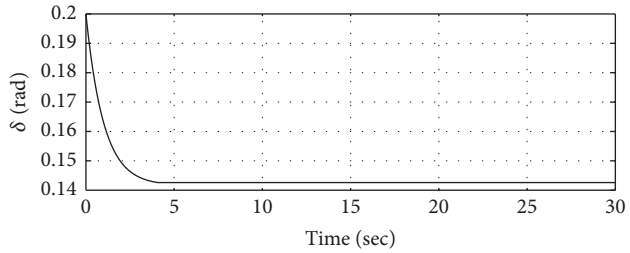

Figure 23: The load phase angle versus time using the first control law (case 3).

initial conditions. We made sure that the discretized model of the power system is chaotic for this initial condition. The simulation results are shown in Figures 23–27. Figures 23–26 show the trajectories of the load phase angle versus time, the load voltage versus time, the generator phase angle versus time, and the generator rotor speed deviation versus time. The errors versus time are shown in Figure 27. It is clear that the errors converge to zero in about 5 seconds. We can conclude that the controller is robust with respect to changes in the initial conditions. Therefore, it can be concluded that the proposed discrete sliding mode controller is able to suppress chaos in the power system. The next section proposes a controller to lessen the chattering problem of this controller.

5. The DSMC Scheme Based on the Double Power Reaching Law

In this section, we will use the double power reaching law [35] to design a discrete sliding mode controller for the discretized model of the chaotic power system. The proposed controller greatly reduces the zigzag motion of the trajectories of the system about the switching surfaces.

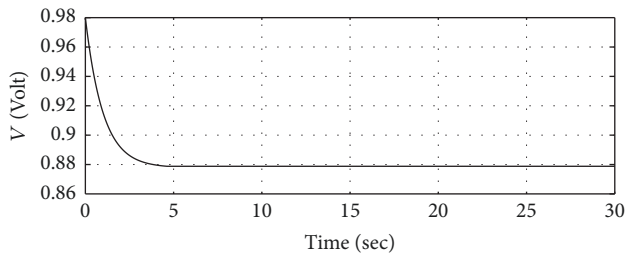

Figure 24: The load voltage versus time using the first control law (case 3).

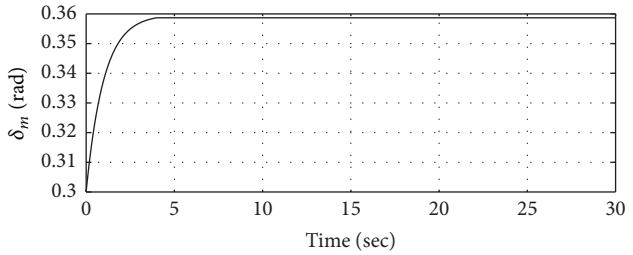

Figure 25: The generator phase angle versus time using the first control law (case 3).

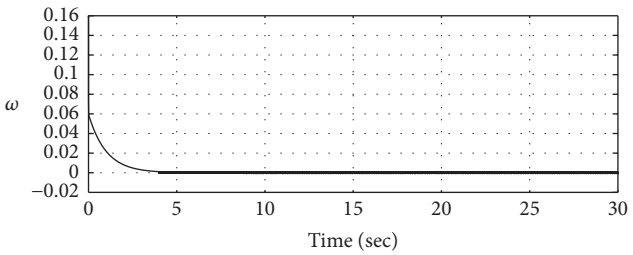

Figure 26: The generator rotor speed deviation versus time using the first control law (case 3).

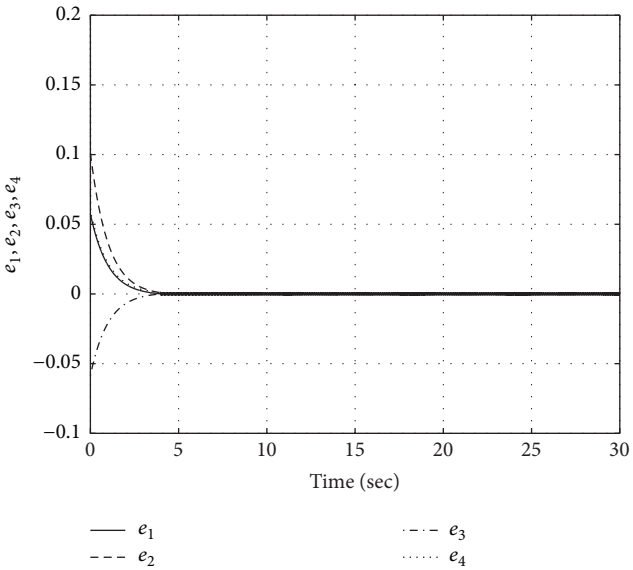

Figure 27: The errors versus time using the first control law (case 3).

5.1. Design of the Controller. The sliding surfaces given by (16) will be used in the design of the second DSMC control scheme.

Let the positive parameters $\epsilon_1, \epsilon_2, q, T_s, \alpha, \beta$ be such that $1 - qT_s > 0$, $0 < \alpha < 1$, and $\beta > 1$. The following proposition gives the second DSMC control scheme.

Proposition 2. *The following sliding mode control scheme*

$$\begin{aligned}
u_1(k) &= (1 - qT_s) S_1(k) - \varepsilon_1 T_s |S_1(k)|^{\alpha} \operatorname{sgn}(S_1(k)) \\
&\quad - \varepsilon_2 T_s |S_1(k)|^{\beta} \operatorname{sgn}(S_1(k)) - e_1(k) - a_1 (e_2(k) \\
&\quad + x_{2d})^2 + a_2 (e_2(k) + x_{2d}) \cos(e_1(k) + x_{1d} \\
&\quad - e_3(k) - x_{3d} - a_3) + a_4 (e_2(k) + x_{2d}) \cos(e_1(k) \\
&\quad + x_{1d} - a_5) + a_6 (e_2(k) + x_{2d}) - a_7 Q_1 - a_8, \\
u_2(k) &= (1 - qT_s) S_2(k) - \varepsilon_1 T_s |S_2(k)|^{\alpha} \operatorname{sgn}(S_2(k)) \\
&\quad - \varepsilon_2 T_s |S_2(k)|^{\beta} \operatorname{sgn}(S_2(k)) - a_{10} (e_2(k) + x_{2d}) \\
&\quad \cdot \cos(e_1(k) + x_{1d} - e_3(k) - x_{3d} - a_{11}) \\
&\quad - a_{12} (e_2(k) + x_{2d}) \cos(e_1(k) + x_{1d} - a_{13}) \\
&\quad - a_{14} (e_2(k) + x_{2d}) + a_{15} Q_1 + a_{16}, \\
u_3(k) &= \frac{1}{T_s} \Big[(1 - qT_s) S_3(k) \\
&\quad - \varepsilon_1 T_s |S_3(k)|^{\alpha} \operatorname{sgn}(S_3(k)) \\
&\quad - \varepsilon_2 T_s |S_3(k)|^{\beta} \operatorname{sgn}(S_3(k)) \Big] + \frac{\gamma - 1}{T_s} (e_3(k) \\
&\quad + T_s e_4(k)) - e_4(k) - a_{17} (e_2(k) + x_{2d}) \sin(e_1(k) \\
&\quad + x_{1d} - e_3(k) - x_{3d} + a_3) + a_{18} e_4(k) - a_{19}
\end{aligned} \tag{29}$$

when applied to the discretized model of the power system (13) guarantees the convergence of the states of the system to their desired values.

Proof. Using the sliding surfaces given by (16), the dynamical model of the errors in (15), and the control scheme given by (29), we obtain

$$\begin{aligned}
S_1(k+1) &= e_1(k+1) = e_1(k) + a_1 (e_2(k) + x_{2d})^2 \\
&\quad - a_2 (e_2(k) + x_{2d}) \\
&\quad \cdot \cos(e_1(k) + x_{1d} - e_3(k) - x_{3d} - a_3) \\
&\quad - a_4 (e_2(k) + x_{2d}) \cos(e_1(k) + x_{1d} - a_5) \\
&\quad - a_6 (e_2(k) + x_{2d}) + a_7 Q_1 + a_8 + u_1(k) \\
&= (1 - qT_s) S_1(k) - \varepsilon_1 T_s |S_1(k)|^{\alpha} \operatorname{sgn}(S_1(k)) \\
&\quad - \varepsilon_2 T_s |S_1(k)|^{\beta} \operatorname{sgn}(S_1(k)),
\end{aligned}$$

$$\begin{aligned}
S_2(k+1) &= e_2(k+1) = -x_{2d} - a_9 (e_2(k) + x_{2d})^2 \\
&\quad + a_{10} (e_2(k) + x_{2d}) \\
&\quad \cdot \cos(e_1(k) + x_{1d} - e_3(k) - x_{3d} - a_{11}) \\
&\quad + a_{12} (e_2(k) + x_{2d}) \cos(e_1(k) + x_{1d} - a_{13}) \\
&\quad + a_{14} (e_2(k) + x_{2d}) - a_{15} Q_1 - a_{16} + u_2(k) \\
&= (1 - qT_s) S_2(k) - \varepsilon_1 T_s |S_2(k)|^{\alpha} \operatorname{sgn}(S_2(k)) \\
&\quad - \varepsilon_2 T_s |S_2(k)|^{\beta} \operatorname{sgn}(S_2(k)), \\
S_3(k+1) &= (1 - \gamma) e_3(k+1) + T_s e_4(k+1) \\
&= (1 - \gamma)(e_3(k) + T_s e_4(k)) \\
&\quad + T_s (e_4(k) - a_{18} e_4(k) + a_{19} + u_3(k)) \\
&\quad + T_s a_{17} (e_2(k) + x_{2d}) \\
&\quad \cdot \sin(e_1(k) + x_{1d} - e_3(k) - x_{3d} + a_3) = (1 - qT_s) \\
&\quad \cdot S_3(k) - \varepsilon_1 T_s |S_3(k)|^{\alpha} \operatorname{sgn}(S_3(k)) - \varepsilon_2 T_s |S_3(k)|^{\beta} \\
&\quad \cdot \operatorname{sgn}(S_3(k)).
\end{aligned} \tag{30}$$

Therefore, (30) can be written as

$$\begin{aligned}
S_i(k+1) &= (1 - qT_s) S_i(k) - \varepsilon_1 T_s |S_i(k)|^{\alpha} \operatorname{sgn}(S_i(k)) \\
&\quad - \varepsilon_2 T_s |S_i(k)|^{\beta} \operatorname{sgn}(S_i(k)) \quad (i = 1\text{–}3).
\end{aligned} \tag{31}$$

Zhao et al. [35] showed that the discrete system described by the difference equation (31) satisfies the two inequalities:

$$\begin{aligned}
(S_i(k+1) - S_i(k)) \operatorname{sgn}(S_i(k)) &< 0, \\
(S_i(k+1) + S_i(k)) \operatorname{sgn}(S_i(k)) &> 0.
\end{aligned} \tag{32}$$

Therefore, it is guaranteed that all the trajectories of system (31) will enter and remain within a domain of decreasing or at the worst case nonincreasing radius. Hence, the discrete system in (31) meets the existence and the reaching condition $|S_i(k+1)| < |S_i(k)|$.

It should be mentioned that Zhao et al. [35] analyzed the reaching rate of the double power reaching law and showed that it possesses better features than those of the conventional exponential reaching law as it reduces the chattering of the trajectories of the controlled system.

Therefore, it can be concluded that $S_1(k)$, $S_2(k)$, and $S_3(k)$ will reach zero in finite time.

On the sliding surfaces, $S_1(k) = 0$, $S_2(k) = 0$, and $S_3(k) = 0$, we have

$$e_1(k) = 0, \tag{33}$$

$$e_2(k) = 0, \tag{34}$$

$$e_3(k) + T_s e_4(k) = \gamma e_3(k). \tag{35}$$

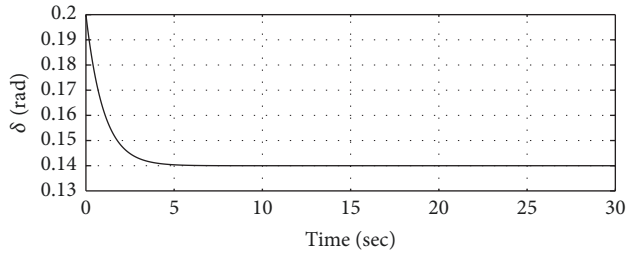

Figure 28: The load angle versus time using the second control law (case 1).

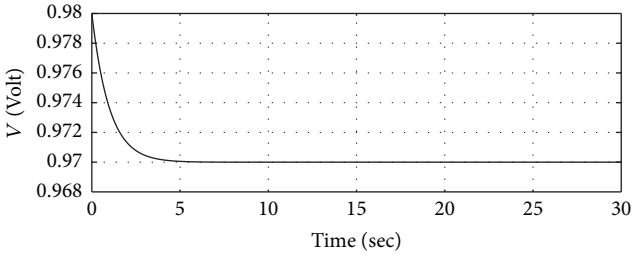

Figure 29: The load voltage versus time using the second control law (case 1).

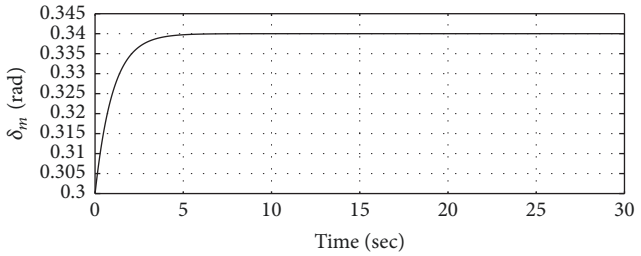

Figure 30: The generator phase angle versus time using the second control law (case 1).

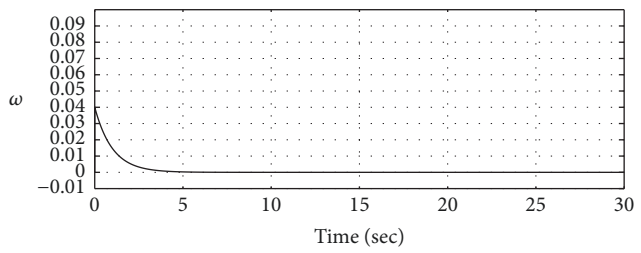

Figure 31: The generator rotor speed deviation versus time using the second control law (case 1).

Using the difference equation given by (35) and the third difference equation of the error system (15), we can write $e_3(k+1) = e_3(k)+T_s e_4(k) = \gamma e_3(k)$. Thus, $e_3(k)$ asymptotically converges to zero as $k \to \infty$ since $|\gamma| < 1$. Also, using (35), it is clear that $e_4(k)$ will converge to zero asymptotically as k tends to ∞.

The convergence of the errors $e_1(k), e_2(k), e_3(k)$, and $e_4(k)$ to zero guarantees that $x_1(k), x_2(k), x_3(k)$, and $x_4(k)$ converge to the desired values x_{1d}, x_{2d}, x_{3d}, and x_{4d}, respectively, as $k \to \infty$. □

5.2. Simulation Results. The designed sliding mode control law in (29) is applied to the discretized model of the chaotic power system given by (13). The performance of the controlled system is simulated using the MATLAB/SIMULINK software. In the simulation, the initial states, the desired states, and the sampling time are taken to be the same as in the previous section. Again, we simulated the performances of the controlled power system for 3 different cases. For the first case, the parameters of the controller are taken to be $q = 1$, $\epsilon_1 = 0.001$, $\epsilon_2 = 0.001$, $\alpha = 0.5$, $\beta = 2$, and $\gamma = 0.1$. The simulation results are shown in Figures 28–35. Figures 28–31 show the trajectories of the load phase angle versus time, the load voltage versus time, the generator phase angle versus time, and the generator rotor speed deviation versus time. The errors versus time are shown in Figure 32. It is clear that the errors converge to zero in about 5 seconds. Therefore, it can be concluded that the proposed discrete sliding mode controller is able to suppress chaos in the power system. In addition, the controllers u_1, u_2, and u_3 versus time are presented in Figures 33–35. It is clear that chattering was greatly reduced. For the second case, the parameters of the controller are taken to be $q = 5$, $\epsilon_1 = 0.01$, $\epsilon_2 = 0.01$, $\alpha = 0.5$, $\beta = 2$, and

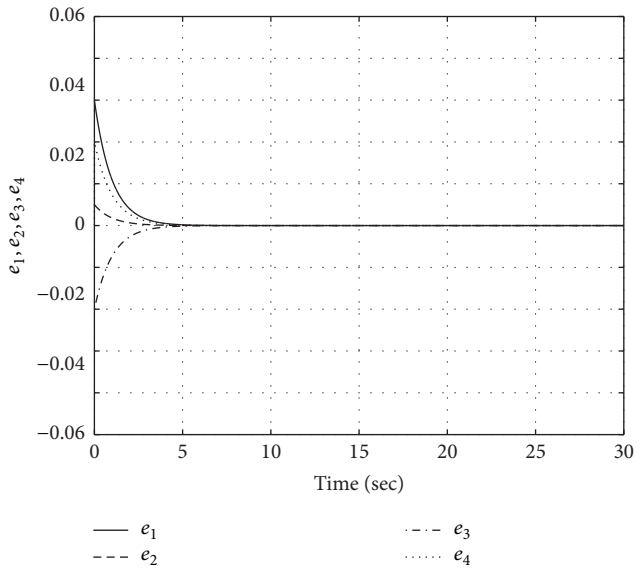

Figure 32: The errors versus time when using the second control law (case 1).

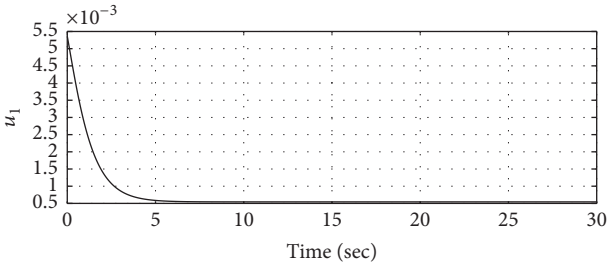

Figure 33: The controller u_1 versus time using the second control law (case 1).

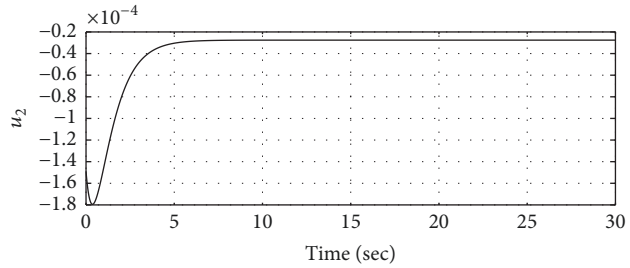

Figure 34: The controller u_2 versus time using the second control law (case 1).

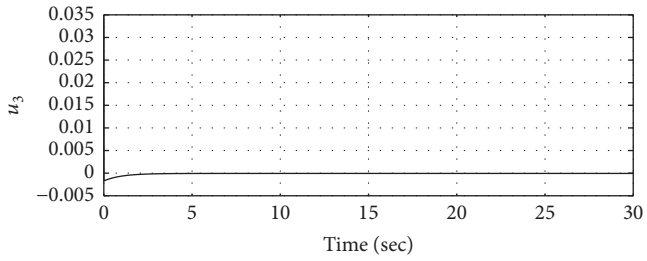

Figure 35: The controller u_3 versus time using the second control law (case 1).

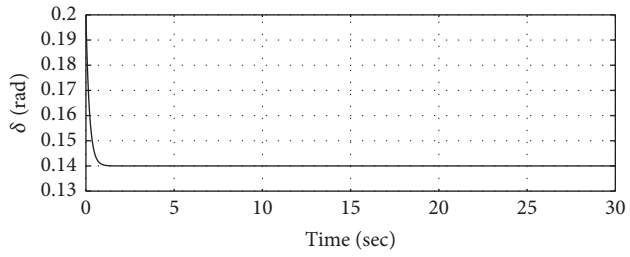

Figure 36: The load angle versus time using the second control law (case 2).

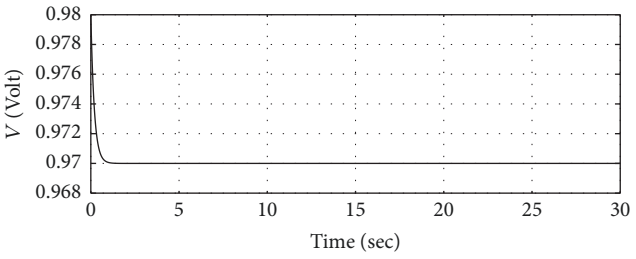

Figure 37: The load voltage versus time using the second control law (case 2).

$\gamma = 0.1$. The simulation results are shown in Figures 36–40. Figures 36–39 show the trajectories of the load phase angle versus time, the load voltage versus time, the generator phase angle versus time, and the generator rotor speed deviation versus time. The errors versus time are shown in Figure 40. It is clear that the errors converge to zero in less than one second. It is noted that the response of the system is faster than the previous case; also chattering was greatly reduced.

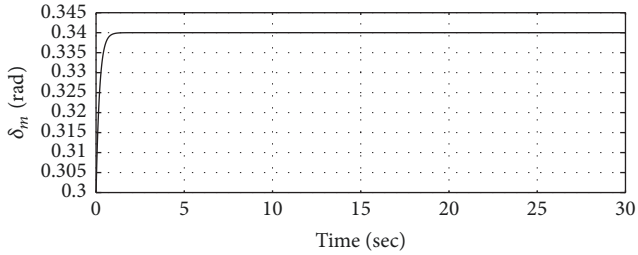

Figure 38: The generator phase angle versus time using the second control law (case 2).

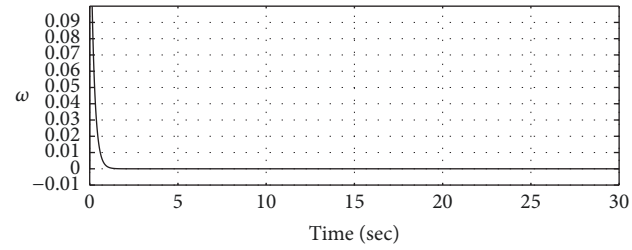

Figure 39: The generator rotor speed deviation versus time using the second control law (case 2).

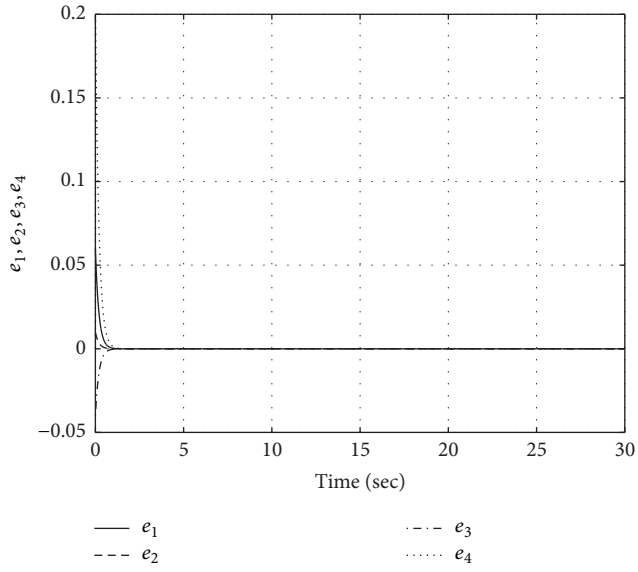

Figure 40: The errors versus time using the second control law (case 2).

For the third case, the parameters of the controller are taken to be $q = 5$, $\epsilon_1 = 0.001$, $\epsilon_2 = 0.001$, $\alpha = 0.5$, $\beta = 2$, and $\gamma = 0.1$. The initial condition of $\omega(t)$ is taken to be $\omega(0) = 0.2$. The simulation results are shown in Figures 41–45. Figures 41–44 show the trajectories of the load phase angle versus time, the load voltage versus time, the generator phase angle versus time, and the generator rotor speed deviation versus time. The errors versus time are shown in Figure 45. It is clear that the errors converge to zero in about 1.5 seconds. We can conclude that the controller is robust with respect to changes in the initial conditions. Therefore, it can be concluded that

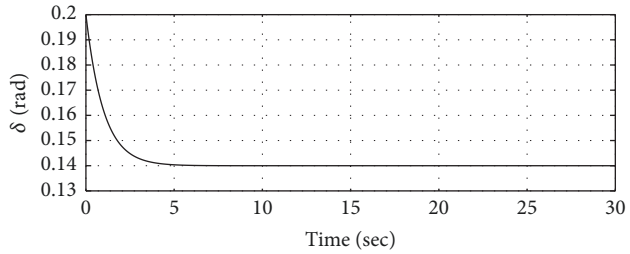

Figure 41: The load angle versus time using the second control law (case 3).

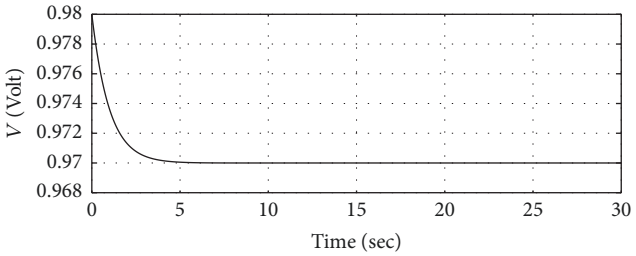

Figure 42: The load voltage versus time using the second control law (case 3).

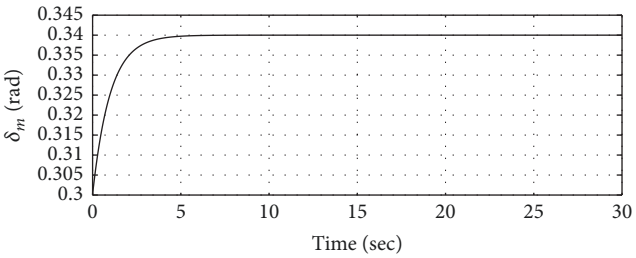

Figure 43: The generator phase angle versus time using the second control law (case 3).

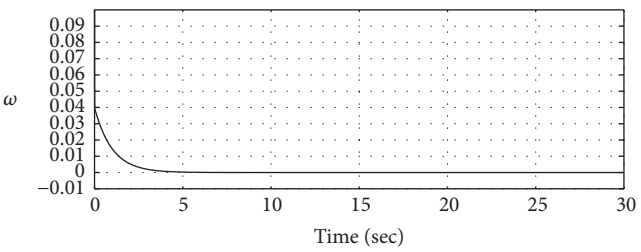

Figure 44: The generator rotor speed deviation versus time using the second control law (case 3).

the proposed second discrete sliding mode controller is able to suppress chaos in the power system.

6. Conclusion

This paper dealt with the suppression of chaos in a discretized model of a chaotic power system. The discrete sliding mode control technique was used. Two controllers were proposed. The first controller uses an exponential reaching law; the second controller uses a double power reaching law. Extensive simulation studies were presented to illustrate the effectiveness of the proposed controllers. The simulation studies show that the two controllers work well. Also, the simulation results indicate that some of the trajectories of the discretized model of the power system when controlled using the first control scheme display zigzag motion about the switching surfaces. However, the second proposed controller greatly reduces the zigzag motion of the trajectories of the system about the switching surfaces. Therefore, the second control scheme gave better results than the first controller. Moreover, simulation studies show that the proposed controllers are robust with respect to changes in the initial conditions.

Future research will tackle the control of chaos in power systems using observer-based sliding mode control schemes.

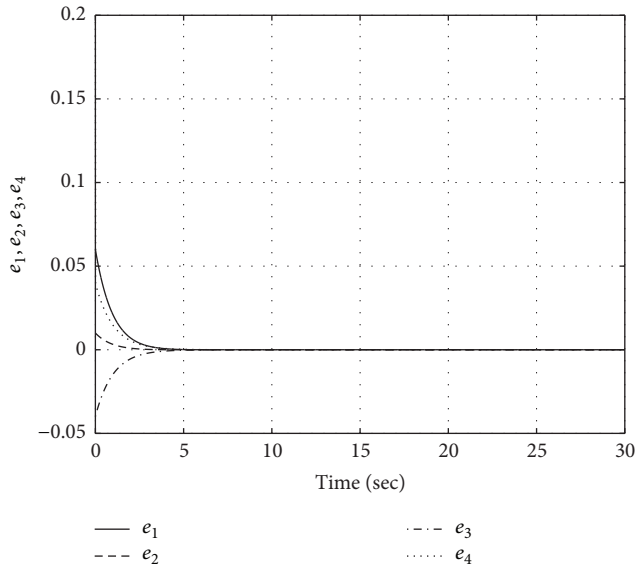

Figure 45: The errors versus time using the second control law (case 3).

Conflicts of Interest

The authors declare that they have no conflicts of interest.

References

[1] H.-D. Chiang, C.-W. Liu, P. P. Varaiya, F. F. Wu, and M. G. Lauby, "Chaos in a simple power system," *IEEE Transactions on Power Systems*, vol. 8, no. 4, pp. 1407–1417, 1993.

[2] H.-D. Chiang, I. Dobson, R. J. Thomas, J. S. Thorp, and L. Fekih-Ahmed, "On Voltage Collapse in Electric Power Systems," *IEEE Transactions on Power Systems*, vol. 5, no. 2, pp. 601–611, 1990.

[3] D. Q. Wei and X. S. Luo, "Noise-induced chaos in single-machine infinite-bus power systems," *EPL (Europhysics Letters)*, vol. 86, no. 5, Article ID 50008, 2009.

[4] D. Q. Wei, B. Zhang, D. Y. Qiu, and X. S. Luo, "Effect of noise on erosion of safe basin in power system," *Nonlinear Dynamics*, vol. 61, no. 3, pp. 477–482, 2010.

[5] Y.-H. Qin, X.-S. Luo, and D.-Q. Wei, "Random-phase-induced chaos in power systems," *Chinese Physics B*, vol. 19, no. 5, Article ID 0505111, 2010.

[6] Y. H. Qin and J. C. Li, "Random parameters induce chaos in power systems," *Nonlinear Dynamics*, vol. 77, no. 4, pp. 1609–1615, 2014.

[7] P. Kundur, "Power System Stability," in *Power System Stability and Control*, L. L. Grigsby, Ed., Electrical Engineering Handbook, CRC Press, 1st edition, 2007.

[8] H. O. Wang, E. H. Abed, and A. M. A. Hamdan, "Bifurcations, chaos, and crises in voltage collapse of a model power system," *IEEE Transactions on Circuits and Systems I: Fundamental Theory and Applications*, vol. 41, no. 4, pp. 294–302, 1994.

[9] C.-W. Tan, M. Varghese, P. Varaiya, and F. F. Wu, "Bifurcation, Chaos, and Voltage Collapse in Power Systems," *Proceedings of the IEEE*, vol. 83, no. 11, pp. 1484–1496, 1995.

[10] A. H. Nayfeh, A. M. Harb, and C.-M. Chin, "Bifurcations in a power system model," *International Journal of Bifurcation and Chaos*, vol. 6, no. 3, pp. 497–512, 1996.

[11] Z. Jing, D. Xu, Y. Chang, and L. Chen, "Bifurcations, chaos, and system collapse in a three node power system," *International Journal of Electrical Power & Energy Systems*, vol. 25, no. 6, pp. 443–461, 2003.

[12] Y. X. Yu, H. J. Jia, P. Li, and J. F. Su, "Power system instability and chaos," *Electric Power Systems Research*, vol. 65, no. 3, pp. 187–195, 2003.

[13] Y. Xu and F. Li, "Adaptive PI control of STATCOM for voltage regulation," *IEEE Transactions on Power Delivery*, vol. 29, no. 3, pp. 1002–1011, 2014.

[14] Q. Y. Sun, Y. G. Wang, J. Yang, Y. Qiu, and H. G. Zhang, "Chaotic dynamics in smart grid and suppression scheme via generalized fuzzy hyperbolic model," *Mathematical Problems in Engineering*, vol. 2014, Article ID 761271, 7 pages, 2014.

[15] I. M. Ginarsa, A. Soeprijanto, and M. H. Purnomo, "Controlling chaos and voltage collapse using an ANFIS-based composite controller-static var compensator in power systems," *International Journal of Electrical Power & Energy Systems*, vol. 46, no. 1, pp. 79–88, 2013.

[16] A. Luo, C. Tang, Z. Shuai, J. Tang, X. Y. Xu, and D. Chen, "Fuzzy-PI-based direct-output-voltage control strategy for the STATCOM used in utility distribution systems," *IEEE Transactions on Industrial Electronics*, vol. 56, no. 7, pp. 2401–2411, 2009.

[17] A. M. Harb and N. Abdel-Jabbar, "Controlling Hopf bifurcation and chaos in a small power system," *Chaos, Solitons & Fractals*, vol. 18, no. 5, pp. 1055–1063, 2003.

[18] A. M. Harb and M. S. Widyan, "Chaos and bifurcation control of SSR in the IEEE second benchmark model," *Chaos, Solitons & Fractals*, vol. 21, no. 3, pp. 537–552, 2004.

[19] D. Q. Wei and X. S. Luo, "Passivity-based adaptive control of chaotic oscillations in power system," *Chaos, Solitons & Fractals*, vol. 31, no. 3, pp. 665–671, 2007.

[20] P. Mercorelli, "An antisaturating adaptive preaction and a slide surface to achieve soft landing control for electromagnetic actuators," *IEEE/ASME Transactions on Mechatronics*, vol. 17, no. 1, pp. 76–85, 2012.

[21] B. Haus, P. Mercorelli, and N. Werner, "A robust adaptive self-tuning sliding mode control for a hybrid actuator in camless internal combustion engines," in *Advances and Applications in Sliding Mode Control Systems*, vol. 576 of *Studies in Computational Intelligence*, pp. 107–136, Springer, 2015.

[22] M. L. Corradini, G. Ippoliti, S. Longhi, and G. Orlando, "A quasi-sliding mode approach for robust control and speed estimation of PM synchronous motors," *IEEE Transactions on Industrial Electronics*, vol. 59, no. 2, pp. 1096–1104, 2012.

[23] S.-C. Tan, Y. M. Lai, and C. K. Tse, "General design issues of sliding-mode controllers in DC–DC converters," *IEEE Transactions on Industrial Electronics*, vol. 55, no. 3, pp. 1160–1174, 2008.

[24] C. Liu, G. Cai, J. Gao, and D. Yang, "Design of nonlinear robust damping controller for power oscillations suppressing based on backstepping-fractional order sliding mode," *Energies*, vol. 10, no. 5, article no. 676, 2017.

[25] E. Nechadi, M. N. Harmas, A. Hamzaoui, and N. Essounbouli, "A new robust adaptive fuzzy sliding mode power system stabilizer," *International Journal of Electrical Power & Energy Systems*, vol. 42, no. 1, pp. 1–7, 2012.

[26] J. Ni, L. Liu, C. Liu, and X. Hu, "Chattering-free time scale separation sliding mode control design with application to power system chaos suppression," *Mathematical Problems in Engineering*, vol. 2016, Article ID 5943934, 14 pages, 2016.

[27] J. Ni, L. Liu, C. Liu, X. Hu, and T. Shen, "Fixed-time dynamic surface high-order sliding mode control for chaotic oscillation in power system," *Nonlinear Dynamics*, vol. 86, no. 1, pp. 401–420, 2016.

[28] C.-Y. Ma, J.-H. Liu, and C.-L. Wang, "Chaos of a power system model and its control," *Journal of Vibration and Control*, vol. 18, no. 14, pp. 2176–2185, 2012.

[29] Y. Niu, D. W. Ho, and Z. Wang, "Improved sliding mode control for discrete-time systems via reaching law," *IET Control Theory & Applications*, vol. 4, no. 11, pp. 2245–2251, 2010.

[30] K. Abidi, J.-X. Xu, and X. Yu,, "On the discrete-time integral sliding-mode control," *IEEE Transactions on Automatic Control*, vol. 52, no. 4, pp. 709–715, 2007.

[31] Y. Zhang and Y.-X. Zhao, "A mixed variable speed reaching law of sliding mode control for spacecraft tracking system," *Mathematical Problems in Engineering*, vol. 2015, Article ID 367146, 10 pages, 2015.

[32] S. C. Qu, X. H. Xia, and J. F. Zhang, "Dynamics of discrete-time sliding-mode-control uncertain systems with a disturbance compensator," *IEEE Transactions on Industrial Electronics*, vol. 61, no. 7, pp. 3502–3510, 2014.

[33] S. Z. Sarpturk, Y. Istefanopulos, and O. Kaynak, "On the stability of discrete-time sliding mode control systems," *IEEE Transactions on Automatic Control*, vol. 32, no. 10, pp. 930–932, 1987.

[34] W. Gao, Y. Wang, and A. Homaifa, "Discrete-time variable structure control systems," *IEEE Transactions on Industrial Electronics*, vol. 42, no. 2, pp. 117–122, 1995.

[35] Y. X. Zhao, T. Wu, and Y. Ma, "A double power reaching law of sliding mode control based on neural network," *Mathematical Problems in Engineering*, vol. 2013, Article ID 408272, 9 pages, 2013.